

Performance analysis of a spectropolarimeter employing a continuous phase variation

Mr. Vasilescu, B.V.; Piron, P.; Loicq, J.J.D.

DOI

[10.1364/OE.487335](https://doi.org/10.1364/OE.487335)

Publication date

2023

Document Version

Final published version

Published in

Optics Express

Citation (APA)

Mr. Vasilescu, B. V., Piron, P., & Loicq, J. J. D. (2023). Performance analysis of a spectropolarimeter employing a continuous phase variation. *Optics Express*, 31(13), 21078-21092.
<https://doi.org/10.1364/OE.487335>

Important note

To cite this publication, please use the final published version (if applicable).
Please check the document version above.

Copyright

Other than for strictly personal use, it is not permitted to download, forward or distribute the text or part of it, without the consent of the author(s) and/or copyright holder(s), unless the work is under an open content license such as Creative Commons.

Takedown policy

Please contact us and provide details if you believe this document breaches copyrights.
We will remove access to the work immediately and investigate your claim.

Green Open Access added to TU Delft Institutional Repository

'You share, we take care!' - Taverne project

<https://www.openaccess.nl/en/you-share-we-take-care>

Otherwise as indicated in the copyright section: the publisher is the copyright holder of this work and the author uses the Dutch legislation to make this work public.

Performance analysis of a spectropolarimeter employing a continuous phase variation

BOGDAN VASILESCU,^{1,*}  PIERRE PIRON,¹ AND JÉRÔME LOICQ^{1,2}

¹*Delft University of Technology, Kluyverweg 1, 2629 HS Delft, Netherlands*

²*University of Liège, Centre Spatial de Liège, Avenue du Pré Aily, 4031 Liège, Belgium*

**B.V.Mr.Vasilescu@tudelft.nl*

Abstract: The light emitted or reflected by a medium can exhibit a certain degree of polarization. Most of the time, this feature brings valuable information about the environment. However, instruments able to accurately measure any type of polarization are hard to build and adapt to inauspicious environments, such as space. To overcome this problem, we presented recently a design for a compact and steady polarimeter, able to measure the entire Stokes vector in a single shot. The first simulations revealed a very high modulation efficiency of the instrumental matrix for this concept. However, the shape and the content of this matrix can change with the characteristics of the optical system, such as the pixel size, the wavelength or the number of pixels. To assess the quality of the instrumental matrices for different optical characteristics, we analyze here the propagation of errors, together with the impact of different types of noise. The results show that the instrumental matrices are converging towards an optimal shape. On this basis, the theoretical limits of sensitivity on the Stokes parameters are inferred.

© 2023 Optica Publishing Group under the terms of the [Optica Open Access Publishing Agreement](#)

1. Introduction

The understanding of reality can be hugely improved with the help of polarization. This property of light, referring to the orientation of the electric field, can be related to many characteristics of the environment. Therefore, with tremendous success, now we use polarization in astronomy [1–3], remote sensing [4], medicine, biology, chemistry, etc. [5–9].

However, despite the large number of applications, the measurement of polarization remains difficult. The main reason for this is the fact that the human eye and the optical detectors are not sensitive to the polarization of light. We need to use special instruments to measure it. These instruments are bulky, very sensitive to the measurement conditions, and only measure a limited set of polarization states.

In recent research, a new method for a non-imaging measurement of polarization was presented [10–12]. As a novelty, this method employs a new type of optical modulator. This component allows for overcoming most of the traditional problems related to polarization measurements. It gives the possibility to build an instrument compact, robust, and suitable even for use in harsh environments, like space. Moreover, it can measure any type of polarization through a single shot.

However, in contrast with the traditional way of measuring polarization, where a limited number of equations are used in the modulation schemes, the new instrument can employ much more equations. Therefore, the instrumental matrix can have a very large format. In addition, this matrix will depend on the geometry of the modulator or on the number of pixels, their size, and the used wavelength. Thus, finding an optimal form for these matrices is no longer easy.

Based on the previous results [10], a specific geometrical configuration can be chosen for the modulator to obtain the highest efficiency of the modulation scheme [13]. This way, only three variables are required in the analysis. The system's quality depends on the number of pixels, their size and the wavelength. Therefore, the theory of the impact of noise [14–17] can be used

for different configurations depending on these variables in order to assess the quality of the instrumental matrices that can be obtained.

This paper uses two main concepts to analyze these matrices: the condition number (*CN*) and the equally weighted variance (*EWV*). The *CN* provides information about how errors are propagated through the instrumental matrix. The *EWV* tells how the retrieved Stokes parameters are impacted by the type of noise. This way, we can see if the proposed instrument behaves or not like an optimal one.

The results of simulations show that, in certain conditions, the instrument is very close to an optimal one. No matter the wavelength, the matrices are converging towards an ideal form. In conclusion, the proposed design not only solves many practical difficulties related to the measurement of polarization, but also provides a very high degree of accuracy.

2. Measurement of polarization

The classical methods for the determination of polarization rely on Stokes formalism and on the Mueller calculus. The Stokes formalism is a straightforward mathematical description of polarization. At the basis is a vector with four parameters, $\vec{S} = (S_0, S_1, S_2, S_3)^T$, that can represent any type of polarization. Here S_0 stands for the total intensity of light, S_1 for the linear horizontal or vertical state of polarization, S_2 for the linear 45° or 135° states, and S_3 for the circular right or left polarization, while T denotes the transposition operator. Finding the four Stokes parameters requires at least four measurements under different configurations of the optical system. The Stokes vector is related to the structure of the system through the Mueller calculus. Therefore, the state of polarization, $\vec{S}_{out} = (S_{out0}, S_{out1}, S_{out2}, S_{out3})^T$, emerging from a system described by a 4×4 Mueller matrix, M , is:

$$\vec{S}_{out} = M \cdot \vec{S}, \quad (1)$$

where \vec{S} is the incoming state of polarization. Given the fact that the detectors are sensitive only to the intensity of light, only the first term of the emerging vector, S_{out0} , must be taken into consideration for the measurement of polarization. Therefore, the detected intensity is:

$$S_{out0} = M_{00}S_0 + M_{01}S_1 + M_{02}S_2 + M_{03}S_3, \quad (2)$$

where $(M_{00}, M_{01}, M_{02}, M_{03})$ are the terms of the first line of the Mueller matrix, M . When the configuration of the system changes, these terms may also change. To simplify the representation of a system that can embrace N configurations, it is useful then to change the notation from M into W , and from S_{out0} to I , so that:

$$\begin{cases} (M_{0i})_k = W_{ki+1} \\ (S_{out0})_k = I_k \end{cases} \quad \text{for } i = 0, \dots, 3; \quad k = 1, \dots, N, \quad (3)$$

where k is the index of the configuration. Consequently, the N equations that allow the measurement of polarization can be written in the following form [13,18]:

$$\begin{pmatrix} I_1 \\ I_2 \\ I_3 \\ \vdots \\ I_N \end{pmatrix} = \begin{pmatrix} W_{11} & W_{12} & W_{13} & W_{14} \\ W_{21} & W_{22} & W_{23} & W_{24} \\ W_{31} & W_{32} & W_{33} & W_{34} \\ \vdots & \vdots & \vdots & \vdots \\ W_{N1} & W_{N2} & W_{N3} & W_{N4} \end{pmatrix} \cdot \begin{pmatrix} S_0 \\ S_1 \\ S_2 \\ S_3 \end{pmatrix}, \quad (4)$$

or, in a more contracted expression:

$$\vec{I} = W \cdot \vec{S}, \quad (5)$$

where \vec{I} is the vector of the detected intensities (i.e. number of photo-electrons), W is the instrumental matrix and \vec{S} is the incoming Stokes vector that must be measured.

If the transition from one configuration to another requires the move or the rotation of certain components of the instrument, then we are dealing with the sequential measurement of polarization. On the other hand, if the different configurations coexist, then we are speaking about the division of amplitude procedure.

If W is an invertible matrix, the Stokes vector is immediately accessible via

$$\vec{S} = W^{-1} \cdot \vec{I}. \quad (6)$$

Because noise is always present in this kind of measurement, increasing the number of lines of the system (Eq. (4)) may help mitigate the influence of spurious signals and enhance the precision of the polarization determination. However, if $N > 4$, then the W matrix is no longer invertible. The only possibility to solve the system (Eq. (5)) is to use the left-inverse matrix, W^\dagger :

$$\begin{cases} W^\dagger = (W^T W)^{-1} W^T \\ W^\dagger W = \mathbb{I}, \end{cases} \quad (7)$$

where T represents the matrix transposition. According to the theory [19], the left inverse matrix exists only if the rank of the matrix $W(N \times 4)$ is equal to 4, when $N \geq 4$. Therefore, the use of the left-inverse matrix should be conditioned by the verification of this necessary and sufficient condition. Multiplying at left side the Eq. (5) with W^\dagger , we obtain

$$\vec{S} = W^\dagger \vec{I}. \quad (8)$$

3. Continuous phase variation spectropolarimeter concept

Most of the classical approaches to generate the W matrix are using the sequential method or the division of amplitude. Therefore, these kinds of instruments often are bulky, limited to certain types of polarization, or not suitable for harsh environments. In this context, we recently presented a new concept of spectropolarimeter able to solve most of these difficulties [10–12]. Using the division of amplitude method, the new instrument allows the full determination of the Stokes vector with a single measurement. Working with a collimated beam, this instrument is adapted for the non-imaging working mode.

The main part of the instrument, the modulator, is composed of three prisms in Magnesium Fluoride (MgF_2), optically glued together and with the fast axis differently oriented in each wedge (see Fig. 1, (a, b)). Therefore, the first prism, (1), of apex angle ξ , has a fast axis oriented along the x -axis. In the middle part of the modulator, (2), the fast axis is oriented along the z -axis, while in the third wedge, (3), of apex angle ψ , the fast axis makes an angle of 45° with the x -axis, in the (xy) -plane. These particular orientations of the fast axes ensure a complete modulation along the vertical direction (i.e. the y -axis) of any incoming state of polarization arriving collimated from the left side of the instrument. Given the variation of the optical thickness along the vertical direction inside the modulator, the phase difference between the two orthogonal components of light varies continuously along the vertical direction. Therefore, a continuous variation of polarization is achieved along the vertical direction on the exit face of the modulator. Because the phase difference induced by the MgF_2 prisms depends also on the birefringence of the material, the modulation of the signal is also spectrally dependent. By placing a linear polarizer after the modulator, with the transmission axis oriented at an angle θ with respect to the horizontal direction, the variation of polarization along the vertical direction can be converted into an

intensity variation, as it is shown in Fig. 1(c). To avoid a high angular separation between the ordinary and extraordinary rays inside the modulator, small values of apex angles must be used. Therefore, the simulations conducted here rely on $\xi = 2.6^\circ$ and $\psi = 1.8^\circ$, whereas the orientation of the analyzer was considered $\theta = 72^\circ$. These values were chosen also in order to ensure a very high efficiency of the modulation scheme [10,13].

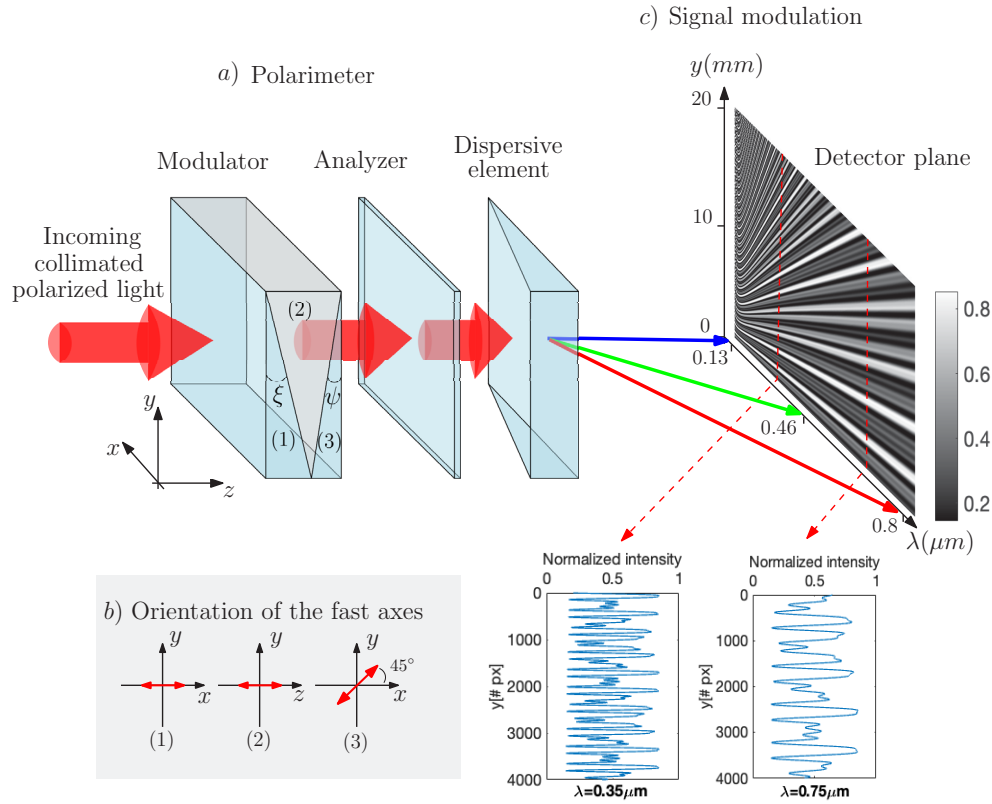


Fig. 1. The general principle of the spectropolarimeter: a) the polarized light arriving collimated from the left side passes through the modulator, the analyzer, and then is dispersed horizontally by a dispersive element. Each prism of the modulator has a particular orientation of the fast axis: along the x axis in (1), along z in (2), and at 45° in (3). The modulation of the signal obtained with this modulator is spectrally dependent (c). The period of the signal increases with the wavelength. In addition, each incoming state of polarization is characterized by a unique pattern of the intensity. An arbitrary state of polarization $\vec{S} = [1, 0.5, 0.4, 0.3]$ was simulated here.

Since the modulation of the signal is spectrally dependent, due to the birefringence of the modulator, (see Fig. 1(c)), a dispersive element can be placed after the analyzer to disperse the light spectrally along the x -axis, orthogonal to the polarimetric modulation. For an incoming Stokes vector, $\vec{S} = (S_0, S_1, S_2, S_3)^T$, the intensity of light in the detector plane is described by the following equation:

$$I(\theta, y, \lambda) = \frac{1}{2} [S_0 + S_1 \cdot m(\theta, y, \lambda) + S_2 \cdot n(\theta, y, \lambda) + S_3 \cdot p(\theta, y, \lambda)] \quad (9)$$

where θ is the angle of the linear analyzer with respect to the x -axis, y is the position in the vertical direction, and λ is the wavelength. The functions m, n, p , computed with the help of the

Mueller calculus, are given by:

$$\begin{cases} m(\theta, y, \lambda) = \cos(2\theta) \cos(\Delta\phi_3) \\ n(\theta, y, \lambda) = \sin(2\theta) \cos(\Delta\phi_1) + \cos(2\theta) \sin(\Delta\phi_1) \sin(\Delta\phi_3) \\ p(\theta, y, \lambda) = \sin(2\theta) \sin(\Delta\phi_1) - \cos(2\theta) \cos(\Delta\phi_1) \sin(\Delta\phi_3) \end{cases}, \quad (10)$$

where $\Delta\phi_1$ and $\Delta\phi_3$ are the phase differences induced by the prisms (1) and (3):

$$\begin{cases} \Delta\phi_1 = \frac{2\pi}{\lambda} \Delta n(\lambda)(h-y) \tan(\xi) \\ \Delta\phi_3 = \frac{2\pi}{\lambda} \Delta n(\lambda)(h-y) \tan(\psi) \end{cases}, \quad (11)$$

in which $\Delta n(\lambda) = |n_o(\lambda) - n_e(\lambda)|$ is the absolute value of the difference between the ordinary and the extraordinary indices of refraction, also called the birefringence of the medium, while h is the height of the modulator.

Discretizing in the vertical direction the height of the ensemble formed by the modulator and the analyzer into N_t pixels of the same size as the detector pixels, Δy , then each small part of this ensemble will act as a polarimeter with a different configuration. Consequently, a column of N_t pixels from the detector plane will record the signal coming from N_t different polarimeters disposed on the same vertical. For a precise wavelength and orientation of the analyzer, the intensity measured by the illuminated pixels is:

$$\underbrace{\begin{pmatrix} I_1 \\ I_2 \\ \vdots \\ I_N \\ \vdots \\ I_{N_t} \end{pmatrix}}_{\vec{I}} = \frac{1}{2} \underbrace{\begin{pmatrix} \int_0^{\Delta y} dy & \int_0^{\Delta y} m(y) dy & \int_0^{\Delta y} n(y) dy & \int_0^{\Delta y} p(y) dy \\ \int_{\Delta y}^{2\Delta y} dy & \int_{\Delta y}^{2\Delta y} m(y) dy & \int_{\Delta y}^{2\Delta y} n(y) dy & \int_{\Delta y}^{2\Delta y} p(y) dy \\ \vdots & \vdots & \vdots & \vdots \\ \int_{(N-1)\Delta y}^{N\Delta y} dy & \int_{(N-1)\Delta y}^{N\Delta y} m(y) dy & \int_{(N-1)\Delta y}^{N\Delta y} n(y) dy & \int_{(N-1)\Delta y}^{N\Delta y} p(y) dy \\ \vdots & \vdots & \vdots & \vdots \\ \int_{(N_t-1)\Delta y}^{N_t\Delta y} dy & \int_{(N_t-1)\Delta y}^{N_t\Delta y} m(y) dy & \int_{(N_t-1)\Delta y}^{N_t\Delta y} n(y) dy & \int_{(N_t-1)\Delta y}^{N_t\Delta y} p(y) dy \end{pmatrix}}_W \cdot \underbrace{\begin{pmatrix} S_0 \\ S_1 \\ S_2 \\ S_3 \end{pmatrix}}_{\vec{S}}. \quad (12)$$

In the following discussions, the number of lines of the instrumental matrix, N , will always satisfy the relation $N \leq N_t$, where $N_t = h/\Delta y$ is the total number of pixels from a column of the detector. The number of pixels N used in the construction of the W matrix can take any value between 4 and N_t . Therefore, using different values of N will not change the received flux per pixel. In addition, the size of the pixel, Δy , will be taken into account by considering the integrated value of the functions m , n , and p over the pixel size (see Eq. (12)). When $N > 4$, W is no longer invertible. However, working with $N > 4$ may help to mitigate the impact of the noise if the W matrix is well-conditioned and close to an optimal one. Therefore, the objective of the current research is to show that the W matrices are converging toward optimal forms for certain couples of the number of pixels, N , and their size, Δy .

4. Tools for the analysis of the instrumental matrix

From the Eqs. (10), (11) and (12) we see that, for a given configuration of the polarimeter (i.e. the angles ξ , ψ and θ , and the height, h), and a given wavelength, the elements of the matrix W , as well as its dimension and other properties are determined by the number of pixels, N , their

size, Δy , and their location in the vertical direction. Therefore, the size of the matrix can span between 4×4 and $4 \times N$. To see if these matrices W , that can be formed, are suitable or not for the retrieval of polarization, we need to assess their "quality". The best "instruments" for this are the condition number and the equally weighted variance [15,20–22]. Both will be analyzed hereafter. The advantage of the condition number is the fact that allows us to observe if the inverse of the W matrix can be computed with accuracy. On the other hand, the equally weighted variance tells us how the retrieval of the Stokes vector is impacted by different types of noise when a certain W matrix is used.

Both concepts, along with the demodulation of the signal, based on Eqs. (6) and (7), are relying on the possibility to compute the inverse of the instrumental matrix, W . As was underlined before, this happens only if the rank of W is 4, for any $N \geq 4$ and for any λ . To have a rank equal to 4, the columns of W should be linearly independent. In addition, more than 4 rows should also be linearly independent. Our previous paper [10], proved that the functions m, n and p are linearly independent. Therefore, the columns of W are also linearly independent. A quick inspection of the Poincaré sphere (see Fig. (2)), where m, n, p are represented on a sphere of radius 1, reveals also that the points $(m(y_i), n(y_i), p(y_i))$, ($i = 1 \dots N$) are covering the entire sphere, for any value of λ . Therefore, the rank of W is 4 and the necessary and sufficient condition for W to have a left-inverse is satisfied. Furthermore, an arbitrary example can be chosen to verify the demodulation procedure based on Eq. (8). Therefore, by considering an incoming normalized Stokes vector $\vec{s} = (1, 1/\sqrt{3}, 1/\sqrt{3}, 1/\sqrt{3})^T$, this procedure was applied to retrieve the polarization, ignoring, at this moment, any other sources of errors. The results (see Fig. (3)) show that for $N > 6$, the relative error on the normalized Stokes parameters is of the order of $6.5 \cdot 10^{-12}$. For $N = 4$, the highest error is observed on s_1 parameter (approximately $5.4 \cdot 10^{-8}$).

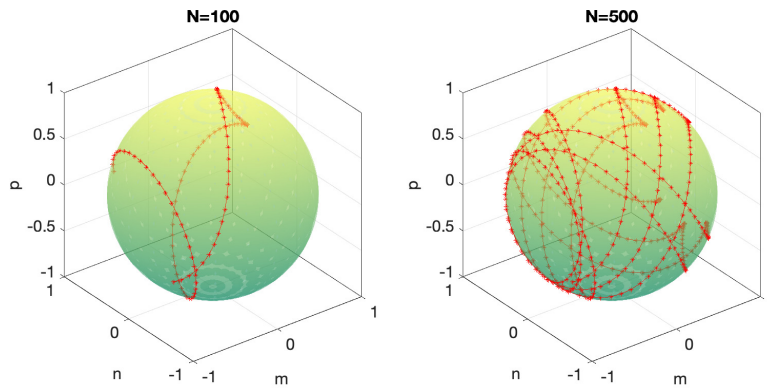


Fig. 2. Poincaré representation of the points $(m(y_i), n(y_i), p(y_i))$, ($i = 1, \dots, N$) on a sphere of radius 1, for two values of N . For these simulations, the size of the pixel was considered to be $\Delta y = 10 \mu\text{m}$ and the wavelength $\lambda = 0.35 \mu\text{m}$.

4.1. Condition number

The condition number provides simultaneously information about how well-conditioned the W matrix is for inversion and how sensitive the system is to changes. Therefore, a small CN indicates a well-conditioned matrix. Small changes in the vector \vec{I} , due to noise, and in the matrix W , due to integration over pixel size, are converted into small variations of the computed Stokes vector \vec{S} with respect to the real incoming state of polarization, \vec{S} . Meanwhile, for an ill-conditioned W matrix, (large CN), small changes of \vec{I} and W generate large changes in the computed state of polarization, \vec{S} [23]. The smallest value of CN is 1 and it corresponds to a unitary matrix, while the highest value is infinity, corresponding to non-invertible matrices. In

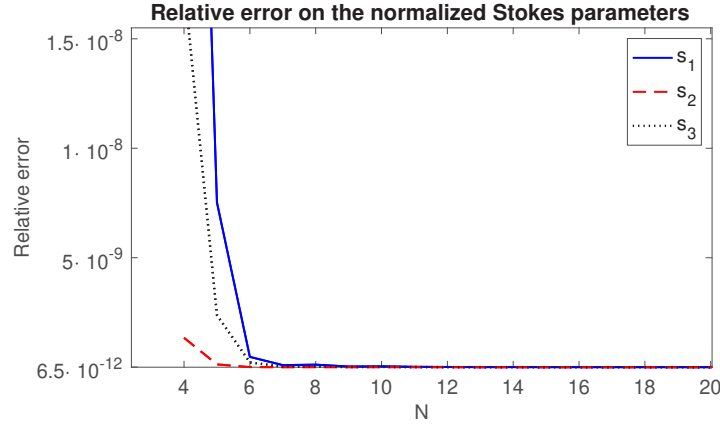


Fig. 3. Relative error on the normalized Stokes parameters as a function of the number of pixels, N . For these simulations, the size of the pixel was considered to be $\Delta y = 10\mu m$, the wavelength, $\lambda = 0.35\mu m$, whereas the incoming normalized polarization was arbitrarily chosen as $\vec{s} = (1, 1/\sqrt{3}, 1/\sqrt{3}, 1/\sqrt{3})^T$.

the case of a polarimeter, where W is no longer a square matrix, the CN is defined as [15,22]:

$$\begin{cases} CN(W) = \|W^\dagger\| \|W\| \\ \|W\| = \sqrt{\text{Tr}(W^T W)} \end{cases}, \quad (13)$$

where Tr is the trace operator. In [22] it was proved that the minimum condition number computed with this formula for an optimal W matrix is $\sqrt{20}$.

4.2. Equally weighted variance

The error on Stokes parameters has two main sources: the algorithm of computation, through the matrix W , and the noise. To mitigate the impact of W , the best strategy is to search for the matrices with the smallest condition number. On the other hand, to assess the impact of noise, the concept of equally weighted variance (EWV) can be used [15,20–22]. When the noise is present in the optical system, Eq. (5) must be adjusted:

$$\vec{I} = W\vec{S} + \vec{B}, \quad (14)$$

where \vec{B} is the noise vector. This noise can be related to the electronics of the instrument, speaking in this case about the Gaussian additive white noise (AWN), or to the number of the received photons, referred to as non-additive Poisson shot noise (PSN). Multiplying at left side with W^\dagger , the previous relation became:

$$\hat{S} = \vec{S} + W^\dagger \vec{B}, \quad (15)$$

where $\hat{S} = W^\dagger \vec{I}$ is the corrupted Stokes vector. Because in our case W can embrace various forms, the purpose is then to see how the precision of the Stokes parameters is impacted by these forms when the different types of noise are present (see Fig. (4)). We can assess this impact with the help of the equally weighted variance. From its definition [20,21,24], the EWV is nothing else but the sum of the variances on the Stokes parameters of the vector \hat{S} ,

$$EWV(W) = \sum_{k=0}^3 \text{var}(\hat{S}_k) = \text{Tr}[\Gamma^{\hat{S}}], \quad (16)$$

where $\Gamma^{\hat{S}}$ is the covariance matrix of \hat{S} .

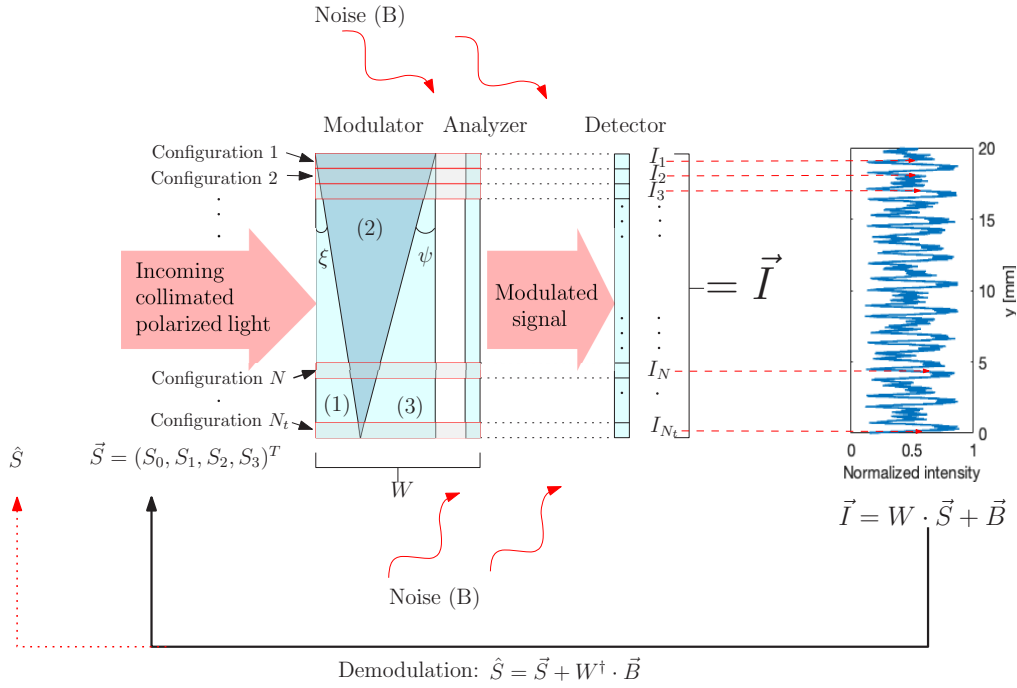


Fig. 4. Schematic representation of the working principle of the polarimeter in the presence of noise, for a single wavelength. The vertical modulation of the signal (\vec{I}), obtained over a column of pixels, is corrupted by the noise \vec{B} . Consequently, the measured state of polarization is \hat{S} instead of \vec{S} . An optimal modulation matrix W allows the minimization of the difference between \hat{S} and \vec{S} .

Therefore, the imprecision on the Stokes parameters and on the degree of polarization can be directly accessed. In the case of a Gaussian white noise of standard deviation σ , EWV becomes

$$EWV(W) = \sigma^2 \text{Tr}[(W^T W)^{-1}], \quad (17)$$

and the minimal values of $EWV(W)$ correspond to optimal W matrices [25]. Previous studies [21,22] have shown that, in the presence of Gaussian noise, for the minimal values of $EWV(W)$, $\Gamma^{\hat{S}}$ has the form

$$\Gamma^{\hat{S}} = \sigma^2 (W^T W)^{-1} = \frac{4}{N} \sigma^2 \begin{pmatrix} 1 & 0 & 0 & 0 \\ 0 & 3 & 0 & 0 \\ 0 & 0 & 3 & 0 \\ 0 & 0 & 0 & 3 \end{pmatrix}, \quad (18)$$

where N is the total number of lines of the matrix W . For this value of $\Gamma^{\hat{S}}$, the EWV is $40\sigma^2/N$.

In the presence of a Poisson, non-additive noise, the expression of the covariance matrix is different as it depends on the intensity, and therefore on the Stokes parameters. In this case, the matrix is given by [14,21]:

$$\Gamma_{ij}^{\hat{S}} = \sum_{k=0}^3 S_k \sum_{n=1}^N W_{in}^\dagger W_{jn}^\dagger W_{nk} \quad \text{for } i, j = 0, \dots, 3. \quad (19)$$

For a design characterized by an optimal modulation scheme, the variances of the Stokes parameters, corresponding to the diagonal terms of the matrix (19) are [21]:

$$\begin{cases} \Gamma_{0,0}^{\hat{S}} = \frac{2S_0}{N} \\ \Gamma_{j,j}^{\hat{S}} = \frac{6S_0}{N}, j = 1, 2, 3 \end{cases} \quad (20)$$

whereas the covariance between S_0 and the rest of the terms is no longer zero. Following Eqs. (13), and (20), the minimum value of the EWV is $20S_0/N$.

5. Optical system analysis

The two concepts previously introduced, for CN and EWV , are hereafter explored while applied to our spectropolarimeter. To simplify the analysis, the structural parameters of the polarimeter are considered fixed. Therefore, the analyzer is oriented at the angle $\theta = 72^\circ$, while the prisms of the modulator, built in MgF_2 , have the apex angles $\xi = 2.6^\circ$, and $\psi = 1.8^\circ$. The only parameters driving the shape of the W matrix for a given wavelength, λ , are in this case the pixel size, Δy , and the number of lines, N , corresponding also to the number of pixels in the vertical direction. As was underlined before, a change in the size or number of pixels is not accompanied here by a variation of the flux. The limits of variation for Δy and N are imposed by the size of the modulator, which is here $2\text{cm} \times 2\text{cm}$. Consequently, the questions that we try to answer here are how many pixels we need to build an optimal modulation matrix and what is the suitable dimension of these pixels.

5.1. Condition number

Using the Eq. (13), the CN was computed for various pixel sizes, Δy , and number of lines, N , of the matrix W . Precise values of the wavelength were arbitrarily chosen within the transmission range of MgF_2 . Therefore, the Fig. (5)-left was plotted for $\lambda = 0.35\mu\text{m}$, and it shows that Δy and N are inversely correlated. An increase of the size of pixel corresponds to a decrease of the number of lines, N , required to obtain the same value of the CN . In addition, it is noticeable that the smallest value of CN is situated between 5 and $\sqrt{20}$, and is reachable for almost any value of the pixel size. This tendency is visible in the Fig. (5)-right. Here, the level of CN was

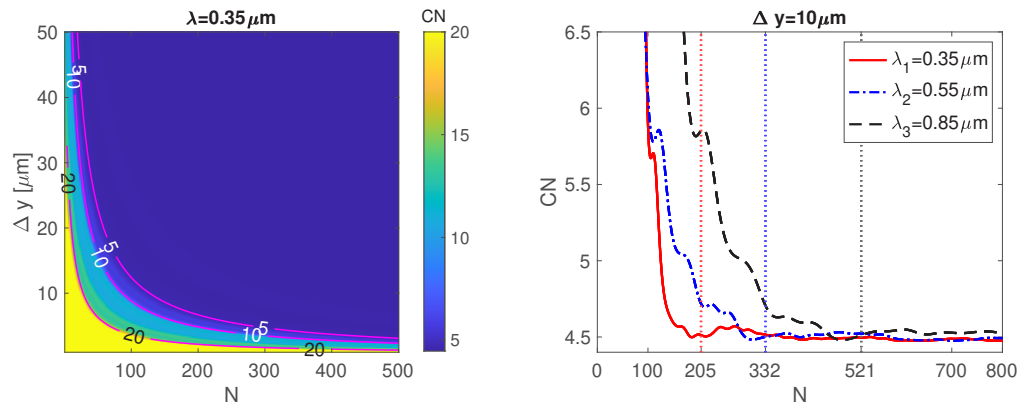


Fig. 5. Left: CN as a function of the pixel size, Δy , and number of lines, N , of the matrix W . For this example, an arbitrary wavelength $\lambda = 0.35\mu\text{m}$ was considered. Level lines corresponding to $CN = 20, 10$ and 5 were also plotted. Right: CN as a function of the number of lines, N , for a pixel size $\Delta y = 10\mu\text{m}$ and three wavelengths. The dotted vertical lines correspond to $\tau_{\max}(\lambda_1)$, $\tau_{\max}(\lambda_2)$, and $\tau_{\max}(\lambda_3)$ respectively.

monitored with respect to the value of N for three different wavelengths. The plot shows that for any wavelength, the CN converges similarly towards the optimal value of $\sqrt{20}$. The only impact of the wavelength is to shift the position of the minimum from where the convergence manifests. Approximately, the convergence occurs after the number of pixels, N , covers along the y -axis a distance equal to the largest period of the functions m, n, p . From Eq. (10) it can be easily shown that this period is:

$$\tau_{max}(\lambda) = \frac{\lambda}{\Delta n(\lambda) \cdot (\tan(\xi) - \tan(\psi))}. \quad (21)$$

6. Equally weighted variance (EWV)

As it was already proved, the notions of condition number and equally weighted variance are closely related [15]. However, the CN only provides information about the propagation of errors through the W matrix. It gives no hint about the level of errors on the Stokes parameters when the noise affects the measurements. For this, the EWV should be studied. This is based on the covariance matrix of the retrieved Stokes vector (see Eq. (16)). Therefore, it can provide information about the variances of the Stokes parameters and about the correlation existing between them.

6.1. Gaussian noise

When the system is subject to the Gaussian noise, the covariance matrix of the Stokes parameters, $\Gamma^{\hat{S}}$, is provided by Eq. (17). In the case of an optimal polarimeter, characterized by an equal impact of the noise on the Stokes parameters, the covariance matrix embraces the form from Eq. (18). Therefore, for such a polarimeter, the variances on S_1, S_2 , and S_3 are three times higher than for the intensity term, S_0 . Because the rest of the matrix is zero, the presence of this noise brings no correlation between the Stokes parameters. Varying one of them will not affect the others.

As we saw in the study of CN , by changing the number of pixels, N , or the size of the pixels on the y direction, Δy , the shape and the "quality" of W can be changed. Thus, by increasing N , we noticed that CN converged towards the optimal value of $\sqrt{20}$. Conducting the same type of simulation for the covariance matrix, we want to see now if this trend can be retrieved again.

To simplify the comparison between the results for our instrument and an optimal case, described by the Eq. (18), we have monitored the evolution of the terms of the matrix G , defined by

$$G = \Gamma^{\hat{S}} \cdot \frac{N}{4\sigma^2}, \quad (22)$$

which is a normalized form of the covariance matrix. Therefore, if the modulation provided by the presented spectropolarimeter converges toward an optimal one, then we should also have:

$$G \xrightarrow{N} \begin{pmatrix} 1 & 0 & 0 & 0 \\ 0 & 3 & 0 & 0 \\ 0 & 0 & 3 & 0 \\ 0 & 0 & 0 & 3 \end{pmatrix}. \quad (23)$$

The upper graph from the Fig. (6) shows that the diagonal terms of the matrix G are converging, with the number of lines N , towards the values 1 and 3. This convergence occurs approximately after $N = 200$. Concerning the rest of the matrix, given the symmetry, only the lower terms are presented in Fig. (6)-bottom. The plots suggest a convergence towards zero. However, for this

trend to manifests, a higher value of N is required. Approximately, this value should satisfy the relation:

$$N \cdot \Delta y > 10 \cdot \tau_{\max}(\lambda). \quad (24)$$

In conclusion, we can say that Eq. (24) is verified for instrumental matrices with a large number of lines. In this case, in the presence of Gauss noise, the studied model of spectropolarimeter behaves like an almost optimal one. By reducing N , the correlation between the Stokes parameters starts to increase. The most affected couples are (S_1, S_2) and (S_1, S_3) . Therefore, despite the fact that such modulation of the intensity allows the retrieval of the polarization state with a number of pixels covering the largest period, $\tau_{\max}(\lambda)$, using a larger number proves to be better in the presence of Gauss noise.

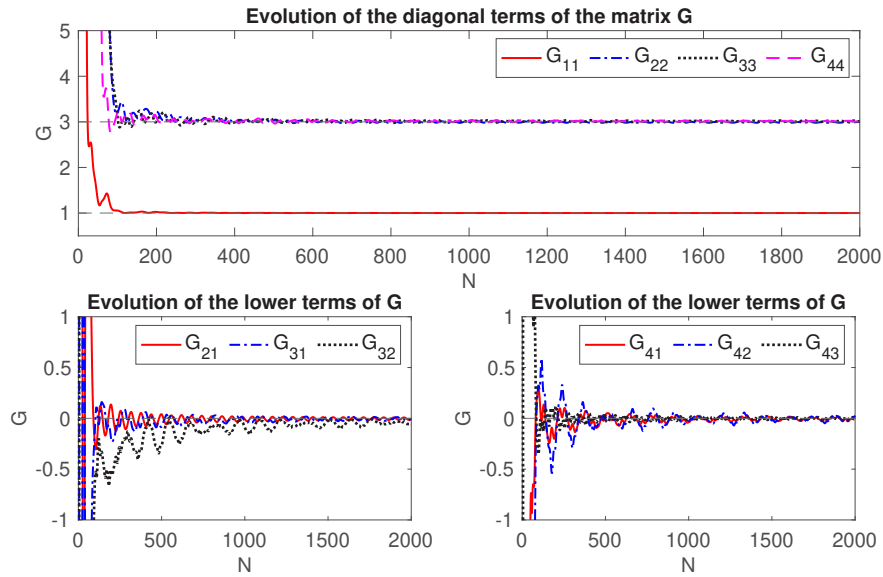


Fig. 6. Gaussian noise: evolution of the terms of the matrix G with the number of lines of the instrumental matrix W . An arbitrary value of the pixel size, $\Delta y = 15\mu\text{m}$, was used for this simulation. The wavelength was set to $0.35\mu\text{m}$. To point out the trend of the G terms, the maximum value of N was fixed now to 2000.

Concerning the value of the EWV , from the Eqs. (16), (17) and (23)) and from the results presented in Fig. (6), we may infer also that:

$$EWV(W(N)) = \frac{40\sigma^2}{N}, \quad (25)$$

for $N \cdot \Delta y > \tau_{\max}(\lambda)$. Therefore, the equally weighted variance also converges towards the optimal value. This trend can be observed in Fig. (7) -left, where EWV was plotted with respect to N for an arbitrary pixel size of $15\mu\text{m}$ and $\lambda = 0.35\mu\text{m}$. The convergence manifests in this case quicker than for the G terms because N is considered in the final expression of the EWV .

6.2. Poisson noise

The non-additive noise is dependent on the level of intensity. For our polarimeter, this level varies from one pixel to another, in the vertical direction, following a sinusoidal shape (see Fig. (1)). Therefore, the noise will vary also in the vertical direction, distorting differently the pattern of intensity from one pixel to another. To assume the impact of this non-additive contribution, the

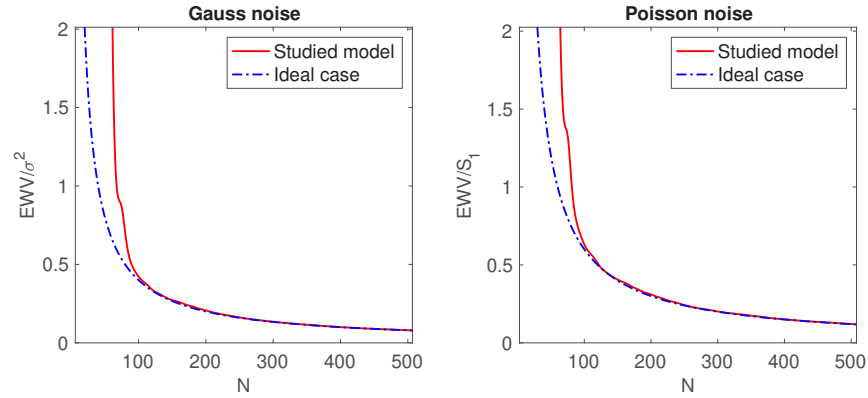


Fig. 7. EWV as a function of the number of lines of the matrix W , for $\Delta y = 15\mu\text{m}$, and $\lambda = 0.35\mu\text{m}$, in the presence of Gaussian noise (left), and Poisson noise (right). The plotted values were normalized by σ , supposed to be constant here, in the case of Gauss noise, and by S_0 , for the Poisson noise.

relations (16) and (19) must be used. It can be noticed that the covariance matrix is different now from the case of the additive noise, as the terms of this matrix are related to the incoming state of polarization.

Using the same procedure as in the case of the Gaussian noise, we have computed the terms of the matrix G , where

$$G = \frac{N}{2S_0} \Gamma^{\hat{S}}, \quad (26)$$

for an arbitrary incoming Stokes vector $\vec{S} = (3, 1.5, 1.4, 1.3)^T$, as a function of the covered distance on the y direction. Because the obtained covariance matrix was proved to be symmetrical, again, only the lower part was presented in Fig. (8). The diagonal terms are showing strong convergence towards the optimal values (see Eq. (20)). However, the rest of the terms are no longer converging towards zero, as in the previous case. A certain trend or average value can be pointed out for each term of the covariance matrix, but the variation around these values is stronger than in the case of additive noise. Using again a large value of N , so that $N \cdot \Delta y \geq 10 \cdot \tau_{\text{max}}$, the covariance matrix becomes, approximately:

$$\Gamma^{\hat{S}} \rightarrow \frac{S_1}{N} \begin{pmatrix} 2 & 1 & 1 & 1 \\ 1 & 6 & 0 & 0 \\ 1 & 0 & 6 & 0 \\ 1 & 0 & 0 & 6 \end{pmatrix}. \quad (27)$$

Just like in the case of the additive noise, the variances on the Stokes parameters are three times higher than for the intensity term. However, the Stokes parameters are no longer uncorrelated now. Therefore, non-diagonal terms of the matrix $\Gamma^{\hat{S}}$ are no longer zero. For small values of N (i.e. $N \cdot \Delta y \leq 10 \cdot \tau_{\text{max}}(\lambda)$), there is also a small correlation between all the Stokes parameters. That means that a variation of one of the Stokes parameters will influence, most likely in a small amount, the value of all the others.

Concerning the equally weighted variance, Fig. (7)-right shows that for $N \cdot \Delta y > \tau_{\text{max}}(\lambda)$ we have a superposition between the studied concept and the values corresponding to an optimal modulation scheme.

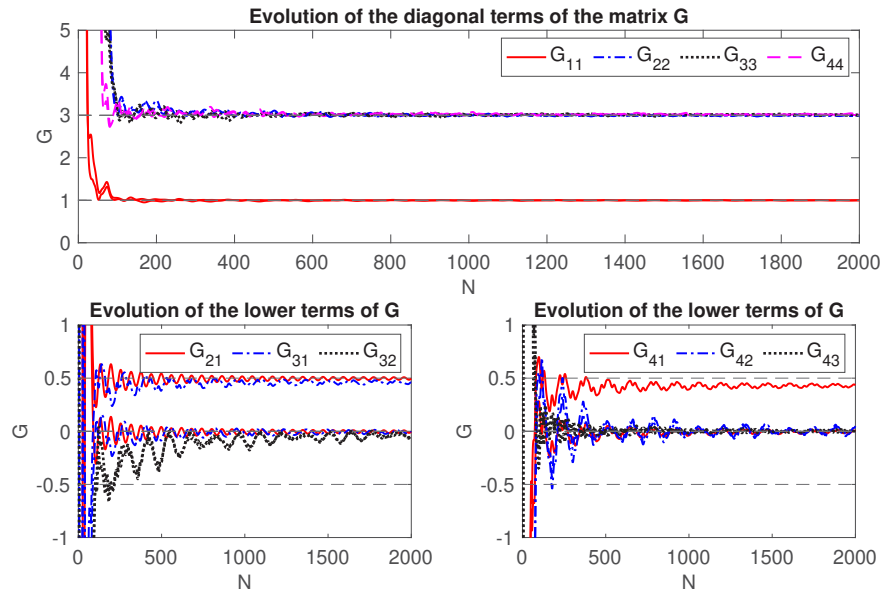


Fig. 8. Diagonal and upper right terms of the covariance matrix in the presence of Poisson noise. The lower-left part of the matrix is identical to the upper-right part, therefore the covariance matrix is diagonal. The simulations correspond to an arbitrary pixel size, $\Delta y = 15\mu\text{m}$, and to a wavelength $\lambda = 0.35\mu\text{m}$.

7. Conclusions

A new concept of spectropolarimeter based on a continuous phase variation was presented here and analyzed from the perspective of the instrumental matrix that is produced. In contrast with the 'traditional' instruments, employing limited and hardly tunable matrices, the instrument presented here allows the construction of various matrices. These matrices may vary in dimension and in the value of each line, according to the sizes of pixels used, and in the number of pixels chosen to extract the polarimetric information.

We have analyzed these matrices from the perspective of the condition number and the equally weighted variance. The condition number was used to assess the propagation of errors through the instrumental matrix. The equally weighted variance showed the impact of different types of noise on the determination of the Stokes vector.

The main parameters used to monitor different instrumental matrices were the number of lines, N , that corresponds also to the number of pixels used to read the signal on the vertical direction, and Δy , the size of the pixel.

For CN , the simulations showed that after a value of N verifying the relation $N \cdot \Delta y = \tau_{\max}(\lambda)$, we have a convergence towards the optimal value of $\sqrt{20}$. In other words, the signal must be read at least over the largest period to achieve this convergence.

Concerning the EWV , the study considered two cases: when the system is affected by the additive Gaussian noise and when it is affected by the non-additive Poisson noise. Because the computation of the EWV is based on the retrieval of the covariance matrix of the measured Stokes parameters, special attention was paid to the latter. Therefore, in the presence of the Gaussian noise, we discovered that the system converges towards an optimal behavior with the number of lines of the instrumental matrix. After approximately $N \cdot \Delta y = 10 \cdot \tau_{\max}(\lambda)$, the covariance matrix can be assimilated to the one corresponding to an optimal modulation scheme. However, when smallest values of N are used, a very small correlation between the Stokes parameters begins

to manifest. The couples (S_1, S_2) and (S_1, S_3) are the most affected. Overall, the covariance on (S_1, S_2, S_3) is three times higher than for the intensity, S_0 . Searching in practice to improve the precision of the Stokes parameters beyond these limits will be impossible.

The system proves to be more sensitive in the presence of the Poisson noise. The covariance matrix also converges towards the optimal one in this case, but the variations around this limit value are higher. For short covered distances ($N \cdot \Delta y < 10 \cdot \tau_{\max}(\lambda)$) all the Stokes parameters prove to be correlated. A small variation of one of them affects all the rest. However, just like in the case of the additive noise, for $N \cdot \Delta y > \tau_{\max}(\lambda)$, the covariance on (S_1, S_2, S_3) is three times higher than for the intensity, S_0 . Because the covariance of the Stokes parameters follow closely the optimal scenario if $N \cdot \Delta y > \tau_{\max}(\lambda)$ for both types of noise, the equally weighted variance converges also towards the optimal value.

In conclusion, this study provided an evaluation of the modulation matrix that can be obtained with our instrument and of the error characterizing the Stokes parameters when the noise is present. We saw that, theoretically, the system can be very close to an optimal one and the limits of precision were inferred.

Still, in a realistic scenario, the modulation in intensity provided by the modulator may drastically differ from the theoretical pattern used during our analysis here. The misalignment of the prisms, of the orientations of the fast axis, or the presence of manufacturing errors related to the size of angles or to the flatness of surfaces may strongly impact the form of the matrix W . Because of this, the study presented here must be doubled by experimental validation. Therefore, laboratory implementation will represent the next step of this research.

Disclosures. The authors declare no conflicts of interest.

Data availability. Data underlying the results presented in this paper are not publicly available at this time but may be obtained from the authors upon reasonable request.

References

1. J. Hough, "Polarimetry: a powerful diagnostic tool in astronomy," *Astron Geophys.* **47**(3), 3.31–3.35 (2006).
2. S. Trippe, "Polarization and polarimetry: a review," *J. The Korean Astron. Soc.* **47**(1), 15–39 (2014).
3. J. Trujillo Bueno, E. Landi Degl'Innocenti, and L. Belluzzi, "The physics and diagnostic potential of ultraviolet spectropolarimetry," *Space Sci. Rev.* **210**(1–4), 183–226 (2017).
4. O. Dubovik, Z. Li, and M. I. Mishchenko, *et al.*, "Polarimetric remote sensing of atmospheric aerosols: Instruments, methodologies, results, and perspectives," *J. Quant. Spectrosc. Radiat. Transf.* **224**, 474–511 (2019).
5. N. Ghosh, "Tissue polarimetry: concepts, challenges, applications, and outlook," *J. Biomed. Opt.* **16**(11), 110801 (2011).
6. D. Ivanov, V. Dreminev, A. Bykov, E. Borisova, T. Genova, A. Popov, R. Ossikovski, T. Novikova, and I. Meglinski, "Colon cancer detection by using Poincaré sphere and 2d polarimetric mapping of *ex vivo* colon samples," *J. Biophotonics* **13**(8), 1 (2020).
7. S. L. Jacques, J. C. Ramella-Roman, and K. Lee, "Imaging skin pathology with polarized light," *J. Biomed. Opt.* **7**(3), 329 (2002).
8. L. Tchvialeva, G. Dhadwal, H. Lui, S. Kalia, H. Zeng, D. I. McLean, and T. K. Lee, "Polarization speckle imaging as a potential technique for *in vivo* skin cancer detection," *J. Biomed. Opt.* **18**(6), 061211 (2012).
9. T. Novikova, A. Pierangelo, A. De Martino, A. Benali, and P. Validire, "Polarimetric imaging for cancer diagnosis and staging," *Opt. Photonics News* **23**(10), 26 (2012).
10. B. Vasilescu, Y. Nazè, and J. Loicq, "Solution uniqueness and noise impact in a static spectropolarimeter based on birefringent prisms for full Stokes parameter retrieval," *J. Astron. Telesc. Instrum. Syst.* **6**(02), 1 (2020).
11. W. Sparks, T. A. Germer, J. MacKenty, and F. Snik, "Compact and robust method for full Stokes spectropolarimetry," *Appl. Opt.* **51**(22), 5495–5511 (2012).
12. M. Pertenais, C. Neiner, P. Bernardi, J.-M. Reess, and P. Petit, "Static spectropolarimeter concept adapted to space conditions and wide spectrum constraints," *Appl. Opt.* **54**(24), 7377–7386 (2015).
13. J. C. del Toro Iniesta and M. Collados, "Optimum modulation and demodulation matrices for solar polarimetry," *Appl. Opt.* **39**(10), 1637 (2000).
14. J. Dai, F. Goudail, M. Boffety, and J. Gao, "Estimation precision of full polarimetric parameters in the presence of additive and Poisson noise," *Opt. Express* **26**(26), 34081 (2018).
15. M. R. Foreman and F. Goudail, "On the equivalence of optimization metrics in Stokes polarimetry," *Opt. Eng.* **58**(08), 1 (2019).

16. D. S. Sabatke, A. M. Locke, M. R. Descour, W. C. Sweatt, J. P. Garcia, E. L. Dereniak, S. A. Kemme, and G. S. Phipps, "Figures of merit for complete Stokes polarimeter optimization," in *Proc. SPIE 4133 Polarization Analysis, Measurement, and Remote Sensing III*, 15 November (2000).
17. D. S. Sabatke, M. R. Descour, E. L. Dereniak, W. C. Sweatt, S. A. Kemme, and G. S. Phipps, "Optimization of retardance for a complete Stokes polarimeter," *Opt. Lett.* **25**(11), 802 (2000).
18. J. C. del Toro Iniesta, *Introduction to Spectropolarimetry* (Cambridge University, 2004).
19. J. Stoer and R. Bulirsch, *Introduction to Numerical Analysis*, vol. 12 of *Texts in Applied Mathematics* (Springer New York, 2002).
20. F. Goudail, "Noise minimization and equalization for Stokes polarimeters in the presence of signal-dependent Poisson shot noise," *Opt. Lett.* **34**(5), 647 (2009).
21. F. Goudail, "Equalized estimation of Stokes parameters in the presence of Poisson noise for any number of polarization analysis states," *Opt. Lett.* **41**(24), 5772 (2016).
22. M. R. Foreman, A. Favaro, and A. Aiello, "Optimal Frames for Polarization State Reconstruction," *Phys. Rev. Lett.* **115**(26), 263901 (2015).
23. E. Cheney and D. Kincaid, *Numerical Mathematics and Computing*, International student edition (Cengage Learning, 2007).
24. A. Bènière, F. Goudail, M. Alouini, and D. Dolfi, "Degree of polarization estimation in the presence of nonuniform illumination and additive Gaussian noise," *J. Opt. Soc. Am. A* **25**(4), 919 (2008).
25. A. Peinado, A. Lizana, J. Vidal, C. Iemmi, and J. Campos, "Optimization and performance criteria of a Stokes polarimeter based on two variable retarders," *Opt. Express* **18**(10), 9815 (2010).